compound pioglitazone could stimulate the circulating CD34$^+$ cells in diabetic patients.

2. Methods

2.1. Study subjects

All subjects gave a written informed consent. The study was approved by the local ethics committee. Thirty-four patients with type 2 diabetes (age 60 ± 10, M/F; 18/16, HbA1c 9.3 ± 1.4%) received 15 or 30 mg pioglitazone for 24 weeks (15 mg; 31 patients, 30 mg; 3 patients). Other medications for diabetes, hypertension and hyperlipidemia were unchanged throughout the study. Insulin was given to 9 patients. Sulfonylurea was given to 15 patients. Biguanide was given to 21 patients. Alpha glucosidase inhibitor was given to 10 patients. Angiotensin converting enzyme inhibitor and/or angiotensin receptor blocker was given to 21 patients. Statin was given to 18 patients. Sixteen patients afflicted with cardiovascular diseases (CVD). Eighteen patients afflicted with nephropathy, 14 patients afflicted with retinopathy, and 15 patients afflicted with neuropathy.

2.2. Measurement of CD34$^+$ cells

Three milliliters of heparinized peripheral blood were obtained after 12-h fasting and measured CD34$^+$ cells. The precise number of circulating CD34$^+$ cells was quantified as we described previously [10]. We evaluated circulating CD34$^+$ cells with Stem-Kit™ (BeckmanCoulter, Marseille, France) according to manufacturers' protocols. These protocols are based on International Society of Hematotherapy and Graft Engineering (ISHAGE) Guidelines [11], and are frequently used for quantification of CD34$^+$ cells mobilized into peripheral blood. To increase the reproducibility of CD34$^+$ cell counts, the protocol of Stem-Kit was modified as follows: the blood sample volume, antibodies and lysing solution were doubled. After adding 30 μl of internal control (Stem count: BeckmanCoulter), samples were centrifuged for 5 min at 450 × *g* and 3860 μl of supernatant was removed carefully with a pipet. Samples were analyzed by Coulter CYTOMICS™ FC500 & XL-system II software (BeckmanCoulter) for 6 min each.

2.3. Other laboratory analysis

Blood samples were taken after 12-h fasting to measure adiponectin and, high sensitive C-reactive protein (hs-CRP) concentrations. Serum adiponectin and concentration was measured by enzyme-linked immunosorbent assay (SRL, Tokyo, Japan). Serum hs-CRP concentration was measured by latex nephelometry method (SRL, Tokyo, Japan). We also measured HbA1c, total cholesterol, HDL cholesterol and triglyceride levels.

2.4. Statistical analysis

Data was expressed using the mean ± S.D. The Student's t-test was used to compare parameter changes over time. The strength of correlation between variables was performed using Spearmann's correlation coefficient.

3. Results

3.1. Effects of pioglitazone on glucose and lipid metabolism

Treatment of pioglitazone significantly decreased HBA1c levels (9.3 ± 1.4, 7.4 ± 1.2 and 7.5 ± 1.7% at 0, 12 and 24 weeks, respectively). Systemic blood pressure levels did not change throughout the study period. BMI did not change throughout the study period (26.8 ± 3.2, 27.5 ± 3.0 and 27.9 ± 3.3 at 0, 12 and 24 weeks, respectively). Total cholesterol and triglyceride levels did not change throughout the study, whereas HDL cholesterol levels significantly increased at 12 and 24 weeks (1.08 ± 0.39, 1.34 ± 0.34 and 1.32 ± 0.28 mmol/l at 0, 12 and 24 weeks, respectively).

3.2. Effects of pioglitazone on adiponectin and inflammatory marker

The inflammatory marker, hs-CRP significantly decreased at 12 and 24 weeks (1518 ± 2350, 840 ± 975, and 838 ± 904 ng/ml at 0, 12, and 24 weeks, respectively). Serum adiponectin levels significantly increased at 12 and 24 weeks (5.0 ± 2.2, 13.5 ± 6.7 and 13.8 ± 8.4 μg/ml at 0, 12 and 24 weeks, respectively). The change in adiponectin levels between 0 and 12 weeks (Δadiponectin) of 30 mg pioglitazone was significantly larger than 15 mg of pioglitazone (15 mg; 7.9 ± 4.7 vs. 30 mg; 19.6 ± 2.5, $p < 0.05$), whereas there was no significant difference in the change in hs-CRP levels (Δhs-CRP) between 15 mg and 30 mg of pioglitazone (15 mg; 267 ± 322 vs. 30 mg; 480 ± 1883).

3.3. Effects of pioglitazone on circulating CD34$^+$ cell level

The number of circulating CD34$^+$ cells significantly increased at 12 and 24 weeks (0.90 ± 0.48, 1.10 ± 0.50, and 1.10 ± 0.57 cells/μl at 0, 12, and 24 weeks, respectively (Fig. 1). This effect was found in both patients with CVD and without CVD (patients with CVD; 0.81 ± 0.51, 1.05 ± 0.46 and 1.04 ± 0.50 cells/μl at 0, 12 and 24 weeks, respectively, $n = 16$, patients without CVD; 0.98 ± 0.41,

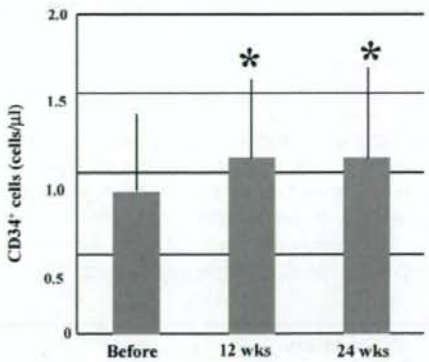

Fig. 1 – CD34+ cell level at 0, 12 and 24 weeks, *$p < 0.05$ vs. 0 week.

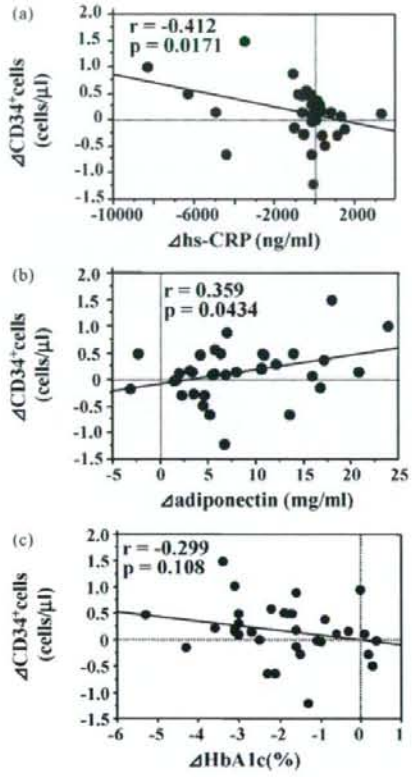

Fig. 2 – Correlation between ΔCD34⁺ cells and ΔhsCRP ($r = -0.412$, $p = 0.017$) (a), correlation between ΔCD34⁺ cells and Δadiponectin ($r = 0.359$, $p = 0.043$) (b), and correlation between ΔCD34⁺ cells and ΔHbA1c ($r = -0.299$, $p = 0.108$) (c).

1.15 ± 0.57 and 1.15 ± 0.65 cells/μl at 0, 12 and 24 weeks, respectively, $n = 18$). There was no significant difference in the change in CD34⁺ cell level (ΔCD34⁺ cells) between 15 mg and 30 mg of pioglitazone (15 mg; 0.07 ± 1.01 vs. 30 mg; 0.14 ± 0.32).

3.4. *Factors involved in the stimulation of CD34⁺ cells*

We next investigated which factors were correlated with the stimulation of CD34⁺ cells. ΔCD34⁺ cells were significantly correlated with Δhs-CRP in univariate analysis ($r = -0.412$, $p = 0.017$) (Fig. 2a). Further, Δadiponectin correlated with Δ CD34⁺ cells ($r = 0.359$, $p = 0.043$) (Fig. 2b). On the other hand, change in HbA1c levels (ΔHbA1c) ($r = -0.299$, $p = 0.108$) (Fig. 2c), change in HDL-C levels (ΔHDL-C) ($r = 0.253$, $p = 0.168$) and change in triglyceride levels (Δtriglycerides) ($r = 0.0072$, $p = 0.969$), were not significantly correlated to Δ CD34⁺ cells.

4. Discussion

Accumulating evidence shows that PPARγ agonists have anti-atherosclerotic actions other than their blood glucose level reduction effects [7,9]. One recent report showed that pioglitazone treatment could stimulate circulating EPCs in patients with coronary artery disease and normal glucose tolerance [12]. In this study, we demonstrated that pioglitazone treatment also increased circulating CD34⁺ cells and this effect continued for 24 weeks in type 2 diabetic patients. We studied the effects of pioglitazone on the stimulation of CD34⁺ cells but not CD34⁺/KDR⁺ cells regarded as EPCs. However, these circulating CD34⁺ cells have the capacity to participate in neovascularization of ischemic tissue. Indeed, their administration enhances the repair of ischemic tissue in ischemic stroke model [13] and improves myocardial circulation in myocardial infarction model [14]. Clinically, circulating CD34⁺ cell levels were reported to be correlated with cerebral blood flow in hypoperfusion area [6] and formation of collateral vessels in stroke patients [15]. These reports suggest that CD34⁺ cells may play a role in the maintenance of microcirculation. One recent clinical trial, PROactive Study, demonstrated that pioglitazone treatment could prevent cardiovascular events including stroke in type 2 diabetic patients [16]. Taken together, it is suggested that the stimulation of CD34⁺ cells may partly contribute to the preventive effects of pioglitazone on cardiovascular diseases. Our study also demonstrated that pioglitazone treatment increased circulating CD34⁺ cells in type 2 diabetic patients irrespective of with or without CVD, suggesting that pioglitazone treatment may be useful for primary prevention as well as secondary prevention of diabetic macroangiopathy.

It has been reported that the number of circulating EPCs is inversely correlated with HbA1c levels [3]. Since pioglitazone treatment significantly decreased HbA1c levels and this study did not have control group, we could not exclude the possibility that the stimulation of CD34⁺ cells was associated with the improvement of glycemic control. However, the results of this study suggest that pioglitazone may be capable of stimulating circulating CD34⁺ cells independently of glycemic control because ΔCD34⁺ cells was not positively correlated with ΔHbA1c at levels that achieved statistical significance.

Adipocyte derived factors and inflammation participate in atherogenesis of type 2 diabetic patients. Accumulating evidence show that adiponectin, one of adipocyte derived factors, has anti-atherogenic properties, and hypoadionectinemia was reported to be associated with endothelial dysfunction [17]. Pioglitazone treatment decreased hs-CRP levels and increased serum adiponectin levels in metabolic syndrome subjects [8], suggesting that these effects contribute to the anti-atherosclerotic action of pioglitazone. In this study, we also demonstrated that pioglitazone treatment decreased hs-CRP levels and increased serum adiponectin levels in type 2 diabetes patients. Interestingly, ΔCD34⁺ cells were significantly correlated with Δhs-CRP and Δadiponectin. An in vitro study showed that CRP impaired EPC migration and function [18]. In clinical study, it has been reported that circulating EPCs were inversely correlated to serum interleukin 6 levels [19]. These reports suggested that chronic inflammation may be involved in the regulation of EPCs. One recent clinical study showed that circulating EPCs were positively correlated to serum adiponectin levels in patients with coronary artery disease [20]. Another report showed that

adiponectin treatment increased EPC number and migration [12]. Taken together, it is suggested that the inhibitory effects on chronic inflammation and the effect on adiponectin regulation of pioglitazone may be directly or indirectly involved in the increase of $CD34^+$ cells. However, further study is necessary to delineate this hypothesis.

In conclusion, our study demonstrated that pioglitazone treatment increased circulating $CD34^+$ cells, suggesting that this effect may at least partly contribute to the anti-atherosclerotic action of pioglitazone.

Conflict of interest

There are no conflicts of interest.

REFERENCES

[1] D.H. Walter, K. Rittig, F.H. Bahlmann, R. Kirchmair, M. Silver, T. Murayama, et al., Statin therapy accelerates reendothelialization: a novel effect involving mobilization and incorporation of bone marrow-derived endothelial progenitor cells, Circulation 105 (2002) 3017–3024.

[2] T. Asahara, T. Murohara, A. Sullivan, Isolation of putative progenitor endothelial cells for angiogenesis, Science 275 (1997) 964–967.

[3] C.J.M. Loomans, E.J.P. de Koning, F.J.T. Staal, M.B. Rookmaaker, C. Verseyden, H.C. de Boer, et al., Endothelial progenitor cell dysfunction: a novel concept in the pathogenesis of vascular complications of type 1 diabetes, Diabetes 53 (2004) 195–199.

[4] M. Majka, A. Janowska-Wieczorek, J. Ratajczak, K. Ehrenman, Z. Pietrzkowski, M.A. Kowalska, et al., Numerous growth factors, cytokines, and chemokines are secreted by human $CD34^+$ cells, myeloblasts, erythroblasts and regulate normal hematopoiesis in an autocrine/paracrine manner, Blood 15 (2001) 3075–3085.

[5] G.P. Fadini, S.V. de Kreutzenberg, A. Coracina, I. Baesso, C. Agostini, A. Tiengo, et al., Circulating CD34+ cells, metabolic syndrome, and cardiovascular risk, Eur. Heart J. 27 (2006) 2247–2255.

[6] A. Taguchi, T. Matsuyama, H. Moriwaki, T. Hayashi, K. Hayashida, K. Nagatsuka, et al., Circulating CD34-positive cells provide an index of cerebrovascular function, Circulation 109 (2004) 2972–2975.

[7] F. Pistorosch, J. Passauer, S. Fischer, In type 2 diabetes, rosiglitazone therapy for insulin resistance ameliorates endothelial dysfunction independent of glucose control, Diabetes Care 27 (2004) 484–490.

[8] K. Esposito, D. Cozzolino, M. Ciotola, D. Carleo, B. Schisano, F. Saccomanno, et al., Effect of rosiglitazone on endothelial function and inflammatory markers in patients with the metabolic syndrome, Diabetes Care 29 (2006) 1071–1076.

[9] F. Blaschke, Y. Takata, E. Caglayan, R.E. Law, W.A. Hsuec, Obesity, peroxisome proliferator-activated receptor, and atherosclerosis in type 2 diabetes, Arteriosc. Thromb. Vasc. Biol. 26 (2006) 28–40.

[10] A. Kikuchi-Taura, T. Soma, T. Matsuyama, D.M. Stern, A. Taguchi, A new protocol for quantifying $CD34^+$ cells in peripheral blood of patients with cardiovascular disease, Texas Heart Inst. J. 33 (2006) 427–429.

[11] D.R. Sutherland, L. Anderson, M. Keeney, R. Nayar, I. Chin-Yee, The ISHAGE guidelines for $CD34^+$ cell determination by flow cytometry. International Society of Hematotherapy and Graft Engineering, J. Hematother. 5 (1996) 213–226.

[12] C. Werner, C.H. Kamani, C. Gensch, M. Bohm, U. Laufs, The peroxisome proliferator-activated receptor-gamma agonist pioglitazone increases number and function of endothelial progenitor cells in patients with coronary artery disease and normal glucose tolerance, Diabetes 56 (2007) 2609–2615.

[13] A. Taguchi, T. Soma, H. Tanaka, T. Kanda, H. Nishimura, H. Yoshikawa, et al., Administration of $CD34^+$ cells after stroke enhances neurogenesis via angiogenesis in a mouse model, J. Clin. Invest. 114 (2004) 330–338.

[14] A. Kawamoto, H. Iwasaki, K. Kusano, T. Murayama, A. Oyamada, M. Silver, et al., CD34-positive cells exhibit increased potency and safety for therapeutic neovascularization after myocardial infarction compared with total mononuclear cells, Circulation 114 (2006) 2163–2169.

[15] T. Yoshihara, A. Taguchi, T. Mastuyama, Y. Shimizu, A. Kikuchi-Taura, T. Soma, et al., Increase in circulating CD34-positive cells in patients with angiographic evidence of moyamoya-like vessels, J. Cereb. Blood Flow Metab. (2008) (e-Pub ahead of print January 2008).

[16] J.A. Dormandy, B. Charbonnel, D.J. Eckland, E. Erdmann, M. Massi-Benedetti, I.K. Moules, et al., Secondary prevention of macrovascular events in patients with type 2 diabetes in the PROactive Study (PROspective pioglitAzone Clinical Trial In macroVascular Events): a randomised controlled trial, Lancet 366 (2005) 1279–1289.

[17] N. Ouchi, M. Ohishi, S. Kihara, T. Funahashi, T. Nakamura, H. Nagaretani, et al., Association of hypoadiponectinemia with impaired vasoreactivity, Hypertension 42 (2003) 231–234.

[18] W. Suh, L. Kim, J.H. Choi, Y.S. Lee, J.Y. Lee, J.M. Kim, et al., C-reactive protein impairs angiogenic functions and decreases the secretion of arteriogenic chemo-cytokines in human endothelial progenitor cells, Biochem. Biophys. Res. Commun. 321 (2004) 65–71.

[19] K. Herbrig, S. Haensel, U. Oelschlaegel, F. Pistrosch, S. Foerster, J. Passauer, Endothelial dysfunction in patients with rheumatoid arthritis is associated with a reduced number and impaired function of endothelial progenitor cells, Ann. Rheum. Dis. 65 (2006) 157–163.

[20] Y. Matsuo, T. Imanishi, A. Kuroi, H. Kitabata, T. Kubo, Y. Hayashi, et al., Effects of plasma adiponectin levels on the number and function of endothelial progenitor cells in patients with coronary artery disease, Circ. J. 17 (2007) 1376–1382.

Journal of Cerebral Blood Flow & Metabolism (2008), 1–4

www.jcbfm.com

Brief Communication

Increase in circulating CD34-positive cells in patients with angiographic evidence of moyamoya-like vessels

Tomoyuki Yoshihara[1], Akihiko Taguchi[1], Tomohiro Matsuyama[2], Yoko Shimizu[1], Akie Kikuchi-Taura[3], Toshihiro Soma[3], David M Stern[4], Hiroo Yoshikawa[5], Yukiko Kasahara[1], Hiroshi Moriwaki[1], Kazuyuki Nagatsuka[1] and Hiroaki Naritomi[1]

[1]*Department of Cerebrovascular Disease, National Cardiovascular Center, Osaka, Japan;* [2]*Institute for Advanced Medical Sciences, Hyogo College of Medicine, Hyogo, Japan;* [3]*Department of Hematology, Osaka Minami National Medical Center, Osaka, Japan;* [4]*Dean's Office, College of Medicine, University of Cincinnati, Cincinnati, Ohio, USA;* [5]*Department of Internal Medicine, Hyogo College of Medicine, Hyogo, Japan*

Increasing evidence points to a role for circulating endothelial progenitor cells, including populations of CD34-positive (CD34$^+$) cells, in maintenance of cerebral blood flow. In this study, we investigated the link between the level of circulating CD34$^+$ cells and neovascularization at ischemic brain. Compared with control subjects, a remarkable increase of circulating CD34$^+$ cells was observed in patients with angiographic moyamoya vessels, although no significant change was observed in patients with major cerebral artery occlusion (or severe stenosis) but without moyamoya vessels. Our results suggest that the increased level of CD34$^+$ cells associated with ischemic stress is correlated with neovascularization at human ischemic brain.
Journal of Cerebral Blood Flow & Metabolism advance online publication, 30 January 2008; doi:10.1038/jcbfm.2008.1

Keywords: antigens; CD34; moyamoya vessel; neovascularization

Introduction

Increasing evidence points to a role for bone marrow-derived immature cells, such as endothelial progenitor cells, in maintenance of vascular homeostasis and repair. CD34-positive (CD34$^+$) cells comprise a population enriched for endothelial progenitor cells whose contribution to neovasculature includes both direct participation in forming the neovessel and regulatory roles as sources of growth/angiogenesis factors (Majka *et al*, 2001). Previously, we have shown accelerated neovascularization after administration of CD34$^+$ cells in an experimental model of stroke (Taguchi *et al*, 2004*b*) and induced by autologous bone marrow mononuclear cells (rich cell fraction of CD34$^+$ cells) transplanted locally into patients with limb ischemia (Taguchi *et al*, 2003). In addition, we have observed a positive correlation between the level of circulating CD34$^+$ cells and regional blood flow (Taguchi *et al*, 2004*a*), and cognitive function (Taguchi *et al*, 2007) in patients with chronic cerebral ischemia.

In this study, we have evaluated the level of circulating CD34$^+$ cells in patients with unusually accelerated neovascularization induced by progressive occlusion (or severe stenosis) of the supraclinoid portion of the internal carotid artery, the proximal region of the anterior, and/or middle cerebral artery characterized angiographically by the presence of moyamoya-like vessels (Natori *et al*, 1997) that supply ischemic brain as collaterals. We have investigated the hypothesis that circulating bone marrow-derived immature cells might be associated with neovascularization at ischemic sites in the human brain.

Patients and methods

The institutional review board of the National Cardiovascular Center approved this study. All subjects provided

Correspondence: Dr A Taguchi, Department of Cerebrovascular Disease, National Cardiovascular Center, 5-7-1 Fujishiro-dai, Suita, Osaka 565-8565, Japan.
E-mail: taguchi@ri.ncvc.go.jp
This work was supported by a Grant-in-Aid for Scientific Research from the Ministry of Health, Labour, and Welfare (H19-Choujyu-029).
Received 29 October 2007; revised 19 December 2007; accepted 26 December 2007

informed consent. A total of 50 individuals, including 24 patients with occlusion or severe stenosis (>90%) at the C1 portion of the internal carotid artery or the M1 portion of the middle cerebral artery, and 26 age-matched healthy volunteers with cardiovascular risk factors, but without history of vascular disease, were enrolled. The diagnosis of cerebral artery occlusion or stenosis was made angiographically and four patients were found to have classical angiographic evidence of moyamoya-like vessels, including one with right C1 occlusion, one with right M1 occlusion, and two with bilateral C1 severe stenosis. All patients with cerebral artery occlusion or stenosis had a history of cerebral infarction. Individuals excluded from the study included patients who experienced a vascular event within 30 days of measurements, premenopausal women, and those with evidence of infection and/or malignant disease. The number of circulating $CD34^+$ cells was quantified as described (Taguchi *et al*, 2007). In brief, blood samples (200 μl) were incubated with phycoerythrin-labeled anti-CD34 antibody, fluorescein isothiocyanate-labeled anti-CD45 antibody, 7-aminoactinomycin-D (7-AAD), and internal control (all of these reagents are in the Stem-Kit; BeckmanCoulter, Marseille, France). After incubation, samples were centrifuged, and supernatant was removed to obtain concentrated cell suspensions. 7-Aminoactinomycin-D-positive dead cells and CD45-negative cells were excluded, and the number of cells forming clusters characteristic of $CD34^+$ cells (i.e., low side scatter and low-to-intermediate CD45 staining) was counted. The absolute number of $CD34^+$ cells was calculated using the internal control. Mean cell number of duplicate measurements was used for quantitative analysis. Statistical comparisons among groups were determined using analysis of variance or χ^2 test. Individual comparisons were performed using a two-tailed unpaired Students' *t*-test or Mann–Whitney's *U*-test. Mean ± s.e. is shown.

Results

Enrolled individuals were divided into three groups: control subjects, patients with cerebral occlusion or severe stenosis, but without the presence of vessels with angiographic characteristics of moyamoya disease, and patients with angiographic evidence of moyamoya-like vessels. Baseline characteristics of the groups are shown in Table 1. The modified Rankin scale evaluation of patients with and without moyamoya-like vessels was 0.5 ± 0.5 and 1.3 ± 0.2, respectively ($P = 0.15$). Comparing these groups, there was a significant difference in the ratio of gender and treatment with aspirin between groups. However, no significant difference was observed in the number of circulating $CD34^+$ cells in control group between genders (male, $n = 13$, $CD34^+$ cells $= 0.93 \pm 0.10/\mu$L; female, $n = 13$, $CD34^+$ cells $= 0.85 \pm 0.11/\mu$L: $P = 0.59$) and treatment with aspirin (aspirin (+), $n = 6$, $CD34^+$ cells $= 0.76 \pm 0.12/\mu$L; aspirin (−), $n = 20$, $CD34^+$ cells $= 0.93 \pm 0.09/\mu$L: $P = 0.26$), indicating mild and nonsignificant effects of gender and treatment with aspirin on the level of circulating $CD34^+$ cells. In univariate analysis of control subjects, each cerebrovascular risk factor and treatment with statins showed no significant difference in the number of circulating $CD34^+$ cells (data not shown).

A representative angiogram showing characteristics of moyamoya-like vessels is shown in Figures 1A and 1B. Angiographic moyamoya-like vessels were observed around the M1 portion of an occluded middle cerebral artery. Compared with a normal subject (Figure 1C) and patients without angiographic evidence of moyamoya-like vessels (Figure 1D), a remarkable increase in levels of

Table 1 Baseline characteristics

	Total	*Control*	*Major artery occlusion/stenosis*		P-*value for trend*
			Moyamoya (−)	*Moyamoya (+)*	
N	50	26	20	4	
Age, years	60.8 ± 1.1	60.5 ± 1.9	61.5 ± 1.0	59.3 ± 5.9	0.85
Male, *n* (%)	33 (66)	13 (50)	18 (90)	2 (50)	0.01
Risk factor, n (%)					
Hypertension	35 (70)	16 (62)	15 (75)	4 (100)	0.24
Hyperlipidemia	26 (52)	14 (54)	10 (50)	2 (50)	0.96
Diabetes mellitus	11 (22)	7 (27)	4 (20)	0 (0)	0.46
Smoking	15 (30)	7 (27)	8 (40)	0 (0)	0.25
Treatment, n (%)					
Ca channel blockers	20 (40)	10 (38)	8 (40)	2 (50)	0.91
β-Blockers	5 (10)	3 (11)	1 (5)	1 (25)	0.44
ACE inhibitor	7 (14)	4 (15)	2 (10)	1 (25)	0.70
ARB	12 (24)	5 (19)	5 (25)	2 (50)	0.40
Diuretics	4 (8)	2 (7)	1 (5)	1 (25)	0.40
Statin therapy	14 (28)	9 (34)	4 (20)	1 (25)	0.54
Aspirin	19 (38)	6 (23)	10 (50)	3 (75)	0.05
Ticlopidine	12 (24)	3 (11)	8 (40)	1 (25)	0.08

Abbreviations: ACE, angiotensin-converting enzyme; ARB, angiotensin 2 receptor blocker.

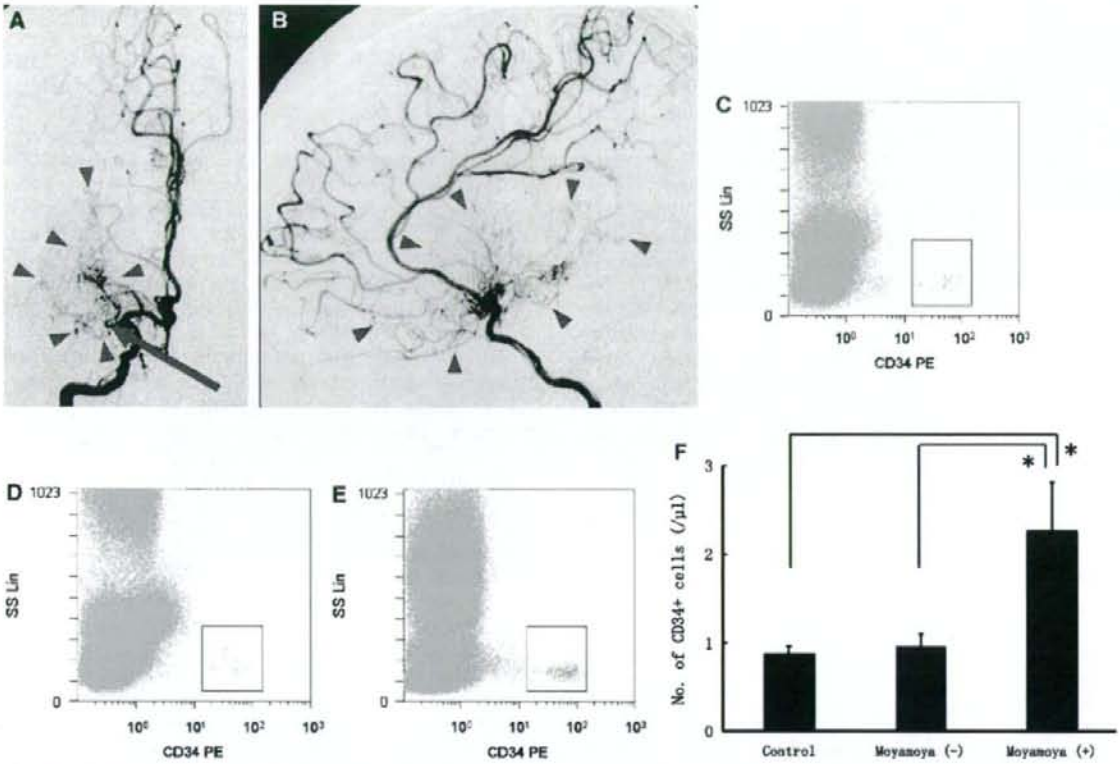

Figure 1 Increased levels of circulating CD34+ cells in patients with angiographic evidence of moyamoya-like vessels. (**A**, **B**) Representative angiogram from a patient with moyamoya-like vessels. Unusually accelerated neovascularization (based on angiographic features of moyamoya-like vessels, arrowheads) was observed around an occlusive M1 lesion (arrow). Anterior–posterior view (**A**) and lateral view (**B**) of the right internal carotid artery showed angiographically. (**C–E**) After exclusion of 7-aminoactinomycin-D (7-AAD)-positive dead cells and CD45-negative cells (nonleukocytes), CD34+ cells cluster at low side scatter. Representative fluorescence-activated cell sorting analyses from a control subject (**C**), a patient without moyamoya-like vessels (**D**), and a patient with moyamoya-like vessels (**E**) are shown. (**F**) A more than two-fold increase in circulating CD34+ cells was observed in patients with moyamoya-like vessels, compared with control subjects and patients without moyamoya-like vessels (*$P < 0.001$). SS Lin: side-scatter linear scale.

peripheral CD34+ cells was observed in patients with moyamoya-like vessels (Figure 1E) based on fluorescence-activated cell sorting. To confirm this impression, levels of circulating CD34+ cells were quantified (control, CD34+ cells $= 0.89 \pm 0.07/\mu$L; moyamoya (−), CD34+ cells $= 0.98 \pm 0.13/\mu$L; moyamoya (+), CD34+ cells $= 2.28 \pm 0.53/\mu$L) and found to be significantly increased in patients with moyamoya-like vessels more than two-fold higher than in controls (Figure 1F, $P < 0.001$).

Discussion

In this study, we have found that a feature of unusually accelerated neovascularization, evidence of moyamoya-like vessels in the immediate locale of an occluded major cerebral artery, can be correlated with a robust increase in the level of circulating CD34+ cells. The latter was determined using a newly developed method that enables quantification of few CD34+ cells in peripheral blood in a highly reproducible manner.

After acute cerebral ischemia, mobilization of CD34+ cells from bone marrow has been shown in stroke patients (Taguchi *et al*, 2004*a*). Furthermore, transplantation of CD34+ cells (Taguchi *et al*, 2004*b*) and bone marrow cells (Borlongan *et al*, 2004*a*, *b*) has been shown to restore cerebral blood flow in experimental models of stroke. In chronic ischemia, transplantation of CD34+ cells has also been shown to accelerate neovascularization, including formation of collateral vessels, in patients with chronic ischemic heart disease (Boyle *et al*, 2006) and limb ischemia (Kudo *et al*, 2003). In addition, there is a report regarding the correlation between inadequate coronary collateral development and reduced numbers of circulating endothelial progenitor cells in

patients with myocardial ischemia (Lambiase *et al*, 2004). In this study, we show, for the first time, a correlation between neovascularization of the cerebral arterial circulation and increased levels of circulating CD34+ cells. Our results support the hypothesis that circulating CD34+ cells potentially contribute to neovascularization at sites of ischemic brain injury.

Acknowledgements

We thank K Obata and Y Okinaka for technical assistance.

Conflict of interest

The authors state no conflict of interest.

References

Borlongan CV, Lind JG, Dillon-Carter O, Yu G, Hadman M, Cheng C, Carroll J, Hess DC (2004*a*) Bone marrow grafts restore cerebral blood flow and blood brain barrier in stroke rats. *Brain Res* 1010:108–16

Borlongan CV, Lind JG, Dillon-Carter O, Yu G, Hadman M, Cheng C, Carroll J, Hess DC (2004*b*) Intracerebral xenografts of mouse bone marrow cells in adult rats facilitate restoration of cerebral blood flow and blood–brain barrier. *Brain Res* 1009:26–33

Boyle AJ, Whitbourn R, Schlicht S, Krum H, Kocher A, Nandurkar H, Bergmann S, Daniell M, O'Day J, Skerrett D, Haylock D, Gilbert RE, Itescu S (2006) Intra-coronary high-dose CD34+ stem cells in patients with chronic ischemic heart disease: a 12-month follow-up. *Int J Cardiol* 109:21–7

Kudo FA, Nishibe T, Nishibe M, Yasuda K (2003) Autologous transplantation of peripheral blood endothelial progenitor cells (CD34+) for therapeutic angiogenesis in patients with critical limb ischemia. *Int Angiol* 22:344–8

Lambiase PD, Edwards RJ, Anthopoulos P, Rahman S, Meng YG, Bucknall CA, Redwood SR, Pearson JD, Marber MS (2004) Circulating humoral factors and endothelial progenitor cells in patients with differing coronary collateral support. *Circulation* 109:2986–92

Majka M, Janowska-Wieczorek A, Ratajczak J, Ehrenman K, Pietrzkowski Z, Kowalska MA, Gewirtz AM, Emerson SG, Ratajczak MZ (2001) Numerous growth factors, cytokines, and chemokines are secreted by human CD34(+) cells, myeloblasts, erythroblasts, and megakaryoblasts and regulate normal hematopoiesis in an autocrine/paracrine manner. *Blood* 97:3075–85

Natori Y, Ikezaki K, Matsushima T, Fukui M (1997) 'Angiographic moyamoya' its definition, classification, and therapy. *Clin Neurol Neurosurg* 99(Suppl 2): S168–72

Taguchi A, Matsuyama T, Moriwaki H, Hayashi T, Hayashida K, Nagatsuka K, Todo K, Mori K, Stern DM, Soma T, Naritomi H (2004*a*) Circulating CD34-positive cells provide an index of cerebrovascular function. *Circulation* 109:2972–5

Taguchi A, Matsuyama T, Nakagomi T, Shimizu Y, Fukunaga R, Tatsumi Y, Yoshikawa H, Kikuchi-Taura A, Soma T, Moriwaki H, Nagatsuka K, Stern DM, Naritomi H (2007) Circulating CD34-positive cells provide a marker of vascular risk associated with cognitive impairment. *J Cereb Blood Flow Metab*; e-pub ahead of print 8 August 2007

Taguchi A, Ohtani M, Soma T, Watanabe M, Kinosita N (2003) Therapeutic angiogenesis by autologous bone-marrow transplantation in a general hospital setting. *Eur J Vasc Endovasc Surg* 25:276–8

Taguchi A, Soma T, Tanaka H, Kanda T, Nishimura H, Yoshikawa H, Tsukamoto Y, Iso H, Fujimori Y, Stern DM, Naritomi H, Matsuyama T (2004*b*) Administration of CD34+ cells after stroke enhances neurogenesis via angiogenesis in a mouse model. *J Clin Invest* 114:330–8

Circulating CD34-Positive Cell Number Is Associated With Brain Natriuretic Peptide Level in Type 2 Diabetic Patients

SADANORI OKADA, MD[1]
HISASHI MAKINO, MD, PHD[1]
AYAKO NAGUMO, MD[1]
TAKAKO SUGISAWA, MD, PHD[1]
MUNEYA FUJIMOTO, MD, PHD[1]
ICHIRO KISHIMOTO, MD, PHD[1]
YOSHIHIRO MIYAMOTO, MD, PHD[1]
AKIE KIKUCHI-TAURA[2]
TOSHIHIRO SOMA, MD[2]
AKIHIKO TAGUCHI, MD, PHD[3]
YASUNAO YOSHIMASA, MD, PHD[1]

Patients with type 2 diabetes often suffer from asymptomatic left ventricular (LV) injury, including increased LV mass, without apparent myocardial ischemia. The mechanisms underlying diabetic LV injury remain unclear; however, it has been suggested that endothelial dysfunction plays a role. Accumulating evidence indicates that bone marrow–derived endothelial progenitor cells (EPCs) contribute to neovascularization of ischemic tissue and endothelialization of denuded endothelium. Recent studies have shown that circulating bone marrow–derived immature cells, including $CD34^+$ cells, contribute to the maintenance of the vasculature, both as a pool of EPCs and as the source of growth/angiogenesis factors (1). We hypothesized that circulating $CD34^+$ cells might be associated with LV dysfunction in patients with type 2 diabetes. Therefore, we studied the correlation between circulating $CD34^+$ cell levels and plasma brain natriuretic peptide (BNP) levels, an LV dysfunction marker, in type 2 diabetic patients.

RESEARCH DESIGN AND METHODS

The institutional review board of the National Cardiovascular Center approved this study, and all subjects provided informed consent. We examined 26 patients with type 2 diabetes (12 men and 14 women, duration of diabetes 16.1 ± 10.7 years) who were over 60 years of age (70.5 ± 6.4 years). Statin was given to nine subjects. ACE inhibitor or angiotensin receptor blocker was given to nine subjects, and thiazolidinedione was given to two subjects. Subjects were excluded from the study if they had known cardiovascular disease or chronic renal failure (defined as serum creatinine ≥180 μmol/l). No study subject showed hypokinesis by echocardiography or electrocardiogram change, indicating myocardial ischemia. Systolic (SBP) and diastolic (DBP) blood pressure and anthropometric parameters were determined. Blood samples were taken after 12-h fasting to measure circulating $CD34^+$ cells, plasma BNP, fasting plasma glucose (FPG), and A1C. Circulating $CD34^+$ cells were quantified by flow cytometry according to the manufacturer's protocol (ProCOUNT; Becton Dickinson Biosciences) as previously reported (2). BNP was quantified by enzyme immunoassay (Tohso, Tokyo, Japan). We further examined LV fractional shortening (LVFS), LV mass index (LVMI) (3), and peak flow velocity of the early filling wave (E), the late filling wave (A), and the E/A-wave ratio (E/A) by echocardiography. All echocardiograms were performed by several expert physicians who were blinded to $CD34^+$ cell level.

All statistical analyses were performed using JMP version 5.1.1 software (SAS Institute). Data are expressed as means ± SD. Comparisons of number of $CD34^+$ cells by sex were made using the two-tailed unpaired *t* test. Correlations between number of $CD34^+$ cells and clinical parameters were assessed by univariate liner regression analysis and multiple regression analysis. LVMI and plasma BNP concentrations were analyzed after logarithmic transformation.

RESULTS

FPG levels, A1C levels, and BMIs in the study subjects were measured to be 9.5 ± 2.6 mmol/l, 9.2 ± 1.8%, and 26.4 ± 4.3 kg/m^2, respectively. A total of 88% of the patients had hypertension (SBP 142 ± 18 mmHg, DBP 75.7 ± 13.5 mmHg). Plasma BNP levels were measured to be 95 ± 319 pg/ml. Although it has been reported that the level of BNP ≥100 pg/ml has a sensitivity of 90% of diagnosing congestive heart failure (CHF) in patients with CHF symptoms (4), none of the subjects in this study, including subjects with ≥100 pg/ml of BNP, showed symptoms of CHF. The level of circulating $CD34^+$ cells was measured to be 0.76 ± 0.39 cells/μl, and there was no significant difference between sexes. The range of LVMI was 73.3–340.2, and 11 subjects applied to the definition of LV hypertrophy (LVMI ≤131 in men and ≤100 in women) (3).

Plasma BNP levels had a significant inverse correlation with the number of circulating $CD34^+$ cells (Fig. 1*A*), whereas FPG, A1C, BMI, SBP, DBP, and age showed no significant correlations. There was a significant correlation between the number of circulating $CD34^+$ cells and LVMI by echocardiography (Fig. 1*B*). LVFS and E/A were not associated with circulating $CD34^+$ cell numbers (LVFS $r = -0.07$, $P = 0.72$; E/A $r = -0.11$, $P = 0.59$). There was also a significant correlation between BNP levels and LVMI ($r = 0.59$, $P = 0.001$).

In multiple regression analysis, the

From the [1]Department of Atherosclerosis, National Cardiovascular Center, Suita, Japan; the [2]Department of Hematology, Osaka Minami National Medical Center, Osaka, Japan; and the [3]Department of Cerebrovascular Disease, National Cardiovascular Center, Suita, Japan.

Address correspondence and reprint requests to Hisashi Makino, MD, Atherosclerosis, National Cardiovascular Center, 5-7-1 Fujishiro-dai, Suita, Osaka 565-8565, Japan. E-mail: makinoh@hsp.ncvc.go.jp.

Received for publication 14 June 2007 and accepted in revised form 13 October 2007.

Published ahead of print at http://care.diabetesjournals.org on 24 October 2007. DOI: 10.2337/dc07-1125.

Abbreviations: BNP, brain natriuretic peptide; CHF, congestive heart failure; DBP, diastolic blood pressure; EPC, endothelial progenitor cell; FPG, fasting plasma glucose; LV, left ventricular; LVFS, LV fractional shortening; LVMI, LV mass index; SBP, systolic blood pressure.

A table elsewhere in this issue shows conventional and Système International (SI) units and conversion factors for many substances.

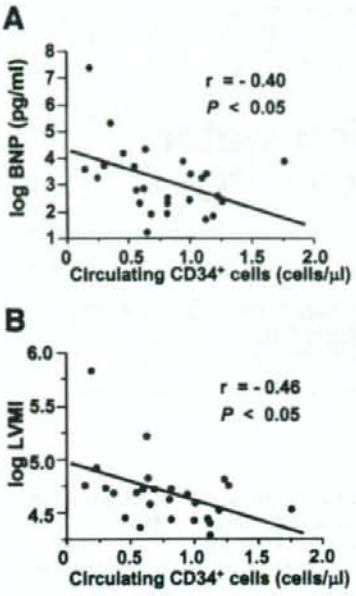

Figure 1—*Correlation between CD34⁺ cell numbers and plasma BNP levels (A) and correlation between CD34⁺ cell numbers and LVMI (B) in type 2 diabetic patients* (n = 26).

level of $CD34^+$ cells was an independent correlate of both BNP ($\beta = -1.64$, $P = 0.017$) and LVMI ($\beta = -0.337$, $P = 0.031$) in the model including age, A1C, SBP, BMI, and medication (ACE inhibitor/angiotensin receptor blocker, statin, and thiazolidinedione).

CONCLUSIONS — In this study, circulating $CD34^+$ cell number was found to significantly correlate with plasma BNP level, a marker of LV dysfunction. To the best of our knowledge, this is the first report that circulating bone marrow–derived cells are associated with diabetic LV abnormality. Circulating $CD34^+$ cell numbers also significantly correlated with LVMI, whereas they did not correlate with LVFS (an LV systolic function marker) or E/A (an LV diastolic function marker). LV hypertrophy is a well-known predictor of cardiovascular events independent of coronary artery disease. The Framingham Heart Study identified an association between diabetes and increased LV wall thickness and mass (5). Although the precise mechanisms underlying the association between diabetes and LV hypertrophy remain unknown, our results suggest that reduced circulating $CD34^+$ cell numbers may be involved in the progression of LV hypertrophy in diabetic patients. However, further investigations are necessary to demonstrate this hypothesis.

We measured the level of $CD34^+$ cells in this study but not the levels of circulating $CD34^+$/kinase insert domain receptor $(KDR)^+$ cells that are regarded as EPCs. Circulating $CD34^+$ cell levels are associated with ischemic stroke (6), and administration of $CD34^+$ cells ameliorates cerebral ischemia in mice (7). This indicates that $CD34^+$ cells may be involved in cardiovascular disease. Indeed, another recent report indicated that levels of circulating $CD34^+$ cells are more strongly correlated with cardiovascular risk than levels of EPCs (8). Therefore, our results suggest that measurement of $CD34^+$ cells may provide an indicator for diabetic LV hypertrophy.

Our study had several limitations. First, the study was performed only by cross-sectional analysis; therefore, a prospective study is needed to clarify whether circulating $CD34^+$ cell numbers predict LV injury in diabetic patients. Second, although systemic blood pressure did not significantly associate with $CD34^+$ cell numbers, further investigation of normotensive diabetic patients is needed to exclude the possible effects of hypertension on circulating $CD34^+$ cell numbers, as most of the subjects in this study were hypertensive. Despite this caveat, these results may be of practical use in elderly patients with type 2 diabetes, as hypertension is a very common comorbid condition in this population.

In conclusion, reduced circulating $CD34^+$ cell numbers are significantly associated with plasma BNP concentration and LVMI in elderly patients with type 2 diabetes. These results suggest that decreased circulating $CD34^+$ cells may be involved in LV hypertrophy and that measurement of circulating $CD34^+$ cell numbers may be useful for the identification of diabetic patients at high risk of LV injury.

References

1. Majka M, Janowska-Wieczorek A, Ratajczak J, Ehrenman K, Pietrzkowski Z, Kowalska MA, Gewirtz AM, Emerson SG, Ratajczak MZ: Numerous growth factors, cytokines, and chemokines are secreted by human CD34(+) cells, myeloblasts, erythroblasts, and megakaryoblasts and regulate normal hematopoiesis in an autocrine/paracrine manner. *Blood* 97:3075–3085, 2001
2. Kikuchi-Taura A, Soma T, Matsuyama T, Stern DM, Taguchi A: A new protocol for quantifying CD34(+) cells in peripheral blood of patients with cardiovascular disease. *Tex Heart Inst J* 33:427–429, 2006
3. Devereux RB, Reichek N: Echocardiographic determination of left ventricular mass in man: anatomic validation of the method. *Circulation* 55:613–618, 1977
4. McCullough PA, Nowak RM, McCord J, Hollander JE, Herrmann HC, Steg PG, Duc P, Westheim A, Omland T, Knudsen CW, Storrow AB, Abraham WT, Lamba S, Wu AHB, Perez A, Clopton P, Krishnaswamy P, Kazanegra R, Maisel AS, BNP multinational study investigators: B-type natriuretic peptide and clinical judgment in emergency diagnosis of heart failure: analysis from Breathing Not Properly (BNP) Multinational Study. *Circulation* 106: 416–422, 2002
5. Galderisi M, Anderson KM, Wilson PW, Levy D: Echocardiographic evidence for existence of a distinct diabetic cardiomyopathy (the Framingham Heart Study). *Am J Cardiol* 68:85–89, 1991
6. Taguchi A, Matsuyama T, Moriwaki H, Hayashi T, Hayashida K, Nagatsuka K, Todo K, Mori K, Stern DM, Soma T, Naritomi H: Circulating CD34-positive cells provide an index of cerebrovascular function. *Circulation* 109:2972–2975, 2004
7. Taguchi A, Soma T, Tanaka H, Kanda T, Nishimura H, Yoshikawa H, Tsukamoto Y, Iso H, Fujimori Y, Stern DM, Naritomi H, Matsuyama T: Administration of CD34+ cells after stroke enhances neurogenesis via angiogenesis in a mouse model. *J Clin Invest* 114:330–338, 2004
8. Fadini GP, de Kreutzenberg SV, Coracina A, Baesso I, Agostini C, Tiengo A, Avogaro A: Circulating CD34+ cells, metabolic syndrome, and cardiovascular risk. *Eur Heart J* 27:2247–2255, 2006

Journal of Cerebral Blood Flow & Metabolism (2008), 1–10

www.jcbfm.com

A physiologic model for recirculation water correction in $CMRO_2$ assessment with $^{15}O_2$ inhalation PET

Nobuyuki Kudomi, Takuya Hayashi, Hiroshi Watabe, Noboru Teramoto, Rishu Piao, Takayuki Ose, Kazuhiro Koshino, Youichirou Ohta and Hidehiro Iida

Department of Investigative Radiology, Advanced Medical-Engineering Center, National Cardiovascular Center Research Institute, Osaka, Japan

Cerebral metabolic rate of oxygen ($CMRO_2$) can be assessed quantitatively using $^{15}O_2$ and positron emission tomography. Determining the arterial input function is considered critical with regards to the separation of the metabolic product of $^{15}O_2$ (RW) from a measured whole blood. A mathematical formula based on physiologic model has been proposed to predict RW. This study was intended to verify the adequacy of that model and a simplified procedure applying that model for wide range of species and physiologic conditions. The formula consists of four parameters, including of a production rate of RW (*k*) corresponding to the total body oxidative metabolism ($BMRO_2$). Experiments were performed on 6 monkeys, 3 pigs, 12 rats, and 231 clinical patients, among which the monkeys were studied at varied physiologic conditions. The formula reproduced the observed RW. Greater *k* values were observed in smaller animals, whereas other parameters did not differ amongst species. The simulation showed $CMRO_2$ sensitive only to *k*, but not to others, suggesting that validity of determination of only *k* from a single blood sample. Also, *k* was correlated with $BMRO_2$, suggesting that *k* can be determined from $BMRO_2$. The present model and simplified procedure can be used to assess $CMRO_2$ for a wide range of conditions and species.
Journal of Cerebral Blood Flow & Metabolism advance online publication, 5 November 2008; doi:10.1038/jcbfm.2008.132

Keywords: arterial input; $CMRO_2$; mathematical modeling; recirculation water; PET

Introduction

Cerebral metabolic rate of oxygen ($CMRO_2$) can be quantitatively assessed using ^{15}O-labeled oxygen ($^{15}O_2$) and positron emission tomography (PET). This technique is based on an estimation of influx rate of $^{15}O_2$ to the cerebral tissue from arterial blood. Using information of cerebral blood flow (CBF) that may be obtained either from a separate scan with ^{15}O-labeled water ($H_2^{15}O$) or from the clearance rate $^{15}O_2$ of tissue, the oxygen extraction fraction (OEF) can also be calculated. The arterial input function must be determined before beginning this calculation. More specifically, a metabolic product of $^{15}O_2$ in the arterial blood, as a form of ^{15}O-labeled water (i.e., recirculating ^{15}O-water or RW) needs to be accurately estimated.

The arterial whole blood radioactivity curve can be obtained by measuring the radioactivity concentration of continuously withdrawn whole blood using a monitoring device (Eriksson *et al*, 1988; Eriksson and Kanno, 1991; Votaw and Shulman, 1998; Kudomi *et al*, 2003). Assessment of a time-dependent RW curve may be achieved by separating the plasma from the whole blood samples. This, however, requires labor-intensive procedures of frequent, manual arterial blood samplings, the centrifugation of all collected blood samples, and radioactivity measurements for both whole blood and plasma (Holden *et al*, 1988).

Ohta *et al* (1992) proposed to neglect the component of RW from the arterial input function. This technique fits three parameters of $CMRO_2$, CBF, and

Correspondence: Dr H Iida, Department of Investigative Radiology, Advanced Medical-Engineering Center, National Cardiovascular Center Research Institute, 5-7-1, Fujishirodai, Suita, Osaka 565-8565, Japan.
E-mail: iida@ri.ncvc.go.jp
This study was supported by the Program for Promotion of Fundamental Studies in Health Science of the Organization for Pharmaceutical Safety and Research of Japan, a Grant for Research on Advanced Medical Technology from the Ministry of Health, Labour and Welfare (MHLW), Japan, and by Nakatani Electronic Measuring Technology Association of Japan (NK).
Received 2 May 2005; revised 6 October 2008; accepted 11 October 2008

cerebral blood volume (CBV) to the kinetic $^{15}O_2$ data obtained from a single PET scan after the bolus administration of $^{15}O_2$. To minimize errors which result from neglecting RW, only the initial 3 mins of data after the bolus inhalation of $^{15}O_2$ were used when calculating the parameters. This approach has been applied to evaluate the magnitude of increase in $CMRO_2$ relative to that in CBF during cognitive stimulation tasks (Fujita *et al*, 1999; Vafaee and Gjedde, 2000; Okazawa *et al*, 2001*a*, *b*; Yamauchi *et al*, 2003; Mintun *et al*, 2002), but one of the drawbacks to this technique is the lack of accurate statistics, which is due to the use of a short scan duration.

Iida *et al* (1993) have developed a mathematical formula to predict the production of RW based on a physiologic model, which allows prolongation of the PET acquisition period with an additional statistical accuracy. The formula assumes a fixed rate constant for production of RW from $^{15}O_2$ in the body. This is based on the fact that the observed rate constant did not vary among clinical subjects, and thus causes nonsignificant errors in $CMRO_2$. However, the study is limited only to human subjects studied at rest, and results have not been verified using other species such as rat and mouse (Magata *et al*, 2003; Temma *et al*, 2006; Yee *et al*, 2006). Also, the findings have not been evaluated on humans who are under physiologic stress, though under such conditions the whole-body oxygen consumption is expected to change. Moreover, it is important to extend the approach to physiologically stressed conditions as recent progress for assessing $CMRO_2$ and CBF simultaneously from a short period dynamic scan by using a dual tracer autoradiography (DARG) (Kudomi *et al*, 2005). The DARG has enabled the $^{15}O_2$ PET to assess $CMRO_2$ and CBF simultaneously at various physiologically activated conditions.

The aim of this study is to verify the method used to estimate the arterial RW during the $^{15}O_2$ inhalation for simultaneous determination of $CMRO_2$ and CBF from the rapid procedures of $^{15}O_2$ PET. The feasibility of a simplified procedure is also being investigated. Applicability of this approach was tested for a wide range of species under various physiologic conditions. Experiments were designed to apply for different species as well as different physiologic conditions. A simulation study was also performed to evaluate the level of error sensitivity associated with this approach.

Materials and methods

Theory

Variables used in the recirculating water model are summarized in Table 1. The mathematical model that formulates the time-dependent RW in arterial blood consists of three rate constants: (1) the production rate of RW or k (per min), proportional to oxidative metabolism in the total body system ($BMRO_2$), (2) the forward diffusion rate (k_1, per min) of the metabolized ^{15}O-water between the blood and interstitial spaces in the body, and (3) the backward diffusion rate (k_2, per min) of the metabolized ^{15}O-water between the blood and interstitial spaces in the body. The differential equations for the arterial activity concentration of ^{15}O-water at a time t (secs) ($A_w(t)$, Bq/mL), after the physical decay correction can be expressed as follows (Huang *et al*, 1991):

$$\frac{d}{dt}A_w(t) = k \cdot A_o(t) - k_w \cdot A_w(t) + k_2 \cdot C(t) \quad (1a)$$

$$\frac{d}{dt}C(t) = k_w \cdot A_w(t) - k_2 \cdot C(t) \quad (1b)$$

$$A_t(t) = A_o(t) + A_w(t) \quad (1c)$$

where $A_o(t)$ and $A_t(t)$ denote the radioactivity concentration of the arterial $^{15}O_2$ and the total radioactivity from both

Table 1 Variables used in the recirculating water model

Symbol	*Description*	*Unit*
A_o	Radioactivity concentration of arterial $^{15}O_2$	Bq/mL
A_w	Radioactivity concentration of arterial $H_2^{15}O$	Bq/mL
A_t	Total radioactivity concentration from arterial $^{15}O_2$ and $H_2^{15}O$	Bq/mL
A_{plasma}	Radioactivity concentration of arterial plasma	Bq/mL
C	Activity concentration of $H_2^{15}O$ in peripheral tissue in a body	Bq/mL
Fi_{O_2}	Oxygen concentration in inhaled gas	%
Fe_{O_2}	Oxygen concentration in expired gas	%
k	Production rate of recirculating $H_2^{15}O$	per min
k_{BM}	Production rate of recirculating $H_2^{15}O$ obtained from BM approach	per min
k_w	Forward diffusion rate of $H_2^{15}O$ from blood to body interstitial space	per min
k_2	Backward diffusion rate of $H_2^{15}O$ from blood to body interstitial space	per min
λ	Decay constant of ^{15}O (= 0.00567 per sec)	per sec
v	Stroke volume	mL
p	k_w/k_2	
r	Respiration rate	per min
R	Fractional water content ratio in whole blood to that in the plasma	
R_{O_2}	Rate of oxidative metabolism in the whole-body system	mL/min
Δt	Delayed appearance time of recirculating water	secs
V_{O_2}	Total volume of molecular oxygen in total blood	mL
V_{TB}	Total volume of blood in a body	mL

$^{15}O_2$ and $H_2^{15}O$, respectively. $C(t)$ is an activity concentration of $H_2^{15}O$ in the peripheral tissue of the total body. Assuming a delayed appearance of RW by Δt (Iida *et al*, 1993), the following equation can be obtained:

$$A_w(t+\Delta t) = k(\alpha_1 \cdot A_t(t) \otimes \exp(-\beta_1 t) + \alpha_2 \cdot A_t(t) \otimes \exp(-\beta_2 t)) \quad (2)$$

where $\otimes$ denotes the convolution integral and:

$$\alpha_{1,2} = \frac{a - 2c \pm \sqrt{a^2 - 4b}}{\pm 2\sqrt{a^2 - 4b}}, \quad \beta_{1,2} = \frac{a \pm \sqrt{a^2 - 4b}}{2},$$
$$a = k + k_w + k_w/p, \quad b = k \cdot k_w/p, \quad c = k_w/p, \quad p = k_w/k_2 \quad (3)$$

Following four approaches were performed to determine the rate constants and $A_w(t)$.

Approach by four parameters fitting: Four parameters, k, Δt, k_w, and p $(=k_w/k_2)$, can be determined from the observed RW ($A_w(t)$) and the $A_t(t)$ curves by means of the nonlinear least square fitting (4PF approach).

Approach by one parameter fitting: Once three parameters, Δt, k_w, and p, are fixed by averaging values determined by the 4PF approach, k can then be determined by fitting the Equation 2 to measured $A_w(t)$ from $A_t(t)$ (1PF approach). In this procedure, single datum is sufficient, and thus k can be determined from $A_t(t)$ and the RW counts sampled at a single time point.

Approach from steady-state condition: Similarly to the 1PF procedures, k can be determined from the steady state condition, which is achieved by a continuous administration of $^{15}O_2$ as follows (SS approach). Incorporating the decay constant of ^{15}O ($\lambda = 0.00567$ per secs) into Equations 1a and 1b provides:

$$\frac{d}{dt}A^*_w(t) = k \cdot A^*_o(t) - k_w \cdot A^*_w(t) + k_2 \cdot C^*(t) - \lambda \cdot A^*_w(t) \quad (4a)$$

$$\frac{d}{dt}C^*(t) = k_w \cdot A^*_w(t) - k_2 \cdot C^*(t) - \lambda \cdot C^*(t) \quad (4b)$$

where variables with the symbol * denote that no correction was made for the radioactivity decay of ^{15}O. After continuously administrating $^{15}O_2$, the radioactivity distribution of $A^*_o(t)$, $A^*_w(t)$, and $C^*_t(t)$ reaches a steady state. Thus, the following equations hold:

$$0 = k \cdot A^*_o(t) - k_w A^*_w(t) + k_2 C^*(t) - \lambda A^*_w(t) \quad (5a)$$

$$0 = k_w A^*_w(t) - k_2 C^*(t) - \lambda C^*(t) \quad (5b)$$

Given the values of k_w and k_2 which are determined as averages of 4PF, k can be calculated from the arterial $^{15}O_2$ and $H_2^{15}O$ concentrations at steady state as follows:

$$k = \lambda\left(\frac{k_w + k_2 + \lambda}{k_2 + \lambda}\right)\frac{A^*_w(t)}{A^*_o(t)} \quad (6)$$

Approach by the rate of whole body oxidative metabolism: In this study, an alternative approach is provided to obtain k, from the rate of oxidative metabolism in the whole-body system (BM approach). With this alternative approach, we assume that the production rate of RW or k is proportional to the rate of oxidative metabolism in the whole-body system (i.e., $BMRO_2$ (R_{O_2}, mL/min)). The rate of oxidative metabolism may change dependent on physiologic status of the subject. In addition, we assumed that this index can be defined from the difference of oxygen concentration between inhaled and exhaled trachea air samples. Therefore, the above can be expressed as follows:

$$k = c \cdot \frac{R_{O_2}}{V_{O_2}} \text{ (per min)} \quad (7a)$$

or

$$k_{BM} = \frac{k}{c} = \frac{R_{O_2}}{1.36 \cdot Hb \cdot V_{TB}} \quad (7b)$$

where c is the proportionality constant, k_{BM} the production rate of RW obtained from BM approach, V_{O_2} (mL) the total volume of molecular oxygen in total blood, 1.36 mL/g the amount of oxygen molecules combined with unit mass of hemoglobin, Hb (g/mL) represents the hemoglobin concentration in the arterial blood, and V_{TB} (mL) is the total volume of blood in the body.

Simulation

A series of simulation studies were performed to investigate the effects of errors on estimated $CMRO_2$ value in the model parameters (k, Δt, k_w, and p). In these simulations, a typical arterial blood time activity curve (TAC) of $^{15}O_2$ and $H_2^{15}O$ after DARG protocol (Kudomi *et al*, 2005) obtained in a monkey study was used. RW TACs were generated from the whole blood TAC by assuming baseline values of k as 0.13, 0.11, 0.34, and 0.73 per min, Δt as 20, 11, 5, and 3 secs, k_w as 0.38, 0.43, 0.98, and 0.87 per min, and p as 1.31, 1.01, 0.98, and 0.83, corresponding to humans, pigs, monkeys, and rats, respectively. Tissue TACs were generated by assuming CBF = 50 mL/min per 100 g and OEF = 0.4 ($CMRO_2$ was defined as: $CMRO_2 = CBF \times OEF \times C_aO_2$, where C_aO_2 is the arterial oxygen content. This simulation was intended to investigate magnitude of error as a percentage difference, so that arbitrary value of C_aO_2 was assumed) (Hayashi *et al*, 2003), using a kinetic formula for oxygen and water in the brain tissue (Mintun *et al*, 1984; Shidahara *et al*, 2002; Kudomi *et al*, 2005). $CMRO_2$ values were calculated by the DARG method (Kudomi *et al*, 2005), in which RW TACs were separated from the whole blood by changing k from 0.0 to 1.0 per min, Δt from 0 to 30 secs, k_w from 0.0 to 2.0 per min, and p from 0.0 to 2.0, respectively. Errors in the estimated $CMRO_2$ were presented as a percentage difference from the assumed true values.

Subjects

Subjects consisted of four groups including monkeys, pigs, rats, and clinical patients. Monkeys were six healthy *macaca fascicularis* with body weight of 5.2 ± 0.8 kg and age ranging from 3- to 4-year old. Pigs were three farm pigs

with body weight of 38 ± 9 kg and age from 4 to 12 months. Rats were 12 male Wistar rats with body weight of 300 ± 54 g and age from 7 to 8 weeks. All animals were studied during anesthesia. The animals were maintained and handled in accordance with guidelines for animal research on Human Care and Use of Laboratory Animals (Rockville, National Institute of Health/Office for Protection from Research Risks, 1996). The study protocol was approved by the Subcommittee for Laboratory Animal Welfare of National Cardiovascular Center.

Human data were retrospectively sampled from an existing database at National Cardiovascular Center which documented subjects who underwent PET examination after the ^{15}O-steady-state protocol. There were 231 total samples, with body weight and age ranging from 58 ± 10 kg, and 63 ± 14 years, respectively. Only the arterial $^{15}O_2$ and $H_2^{15}O$ radioactivity concentrations measured at the steady-state condition were used for the present analysis.

Experimental Protocol

The six monkeys were anesthetized using propofol (4 mg/kg/h) and vecuronium (0.05 mg/kg/h) assigned as a baseline in contrast to the after physiologically stimulated conditions. Animals were intubated and their respiration was controlled by an anesthetic ventilator (Cato, Drager, Germany). Each monkey inhaled 2,200 MBq $^{15}O_2$ for 20 secs. After 3 mins, the monkeys were injected with 370 MBq $H_2^{15}O$ for 30 secs by the anterior tibial vein. This was aimed at assessing both CBF and $CMRO_2$ according to the DARG technique (Kudomi *et al*, 2005). At 30 secs before inhaling $^{15}O_2$ to the monkeys, arterial blood was withdrawn from the femoral artery for 420 secs at a rate of 0.45 mL/min using a Harvard pump (Harvard Apparatus, Holliston, MA, USA). The whole blood TAC was measured with a continuous monitoring system (Kudomi *et al*, 2003) and the $A_t(t)$ was obtained. Meanwhile, we also manually obtained 0.5 mL of arterial blood samples from the contralateral femoral artery at 30, 50, 70, 90, 110, 130, 160, 190, and 360 secs after the $^{15}O_2$ inhalation. For the analysis of sampled blood, 0.2 mL of the blood were used for measurement of the radioactivity concentration of the whole blood, and the rest of the blood sampled (~0.3 mL) was immediately centrifuged for separation to measure the plasma radioactivity concentration ($A_{plasma}(t)$, Bq/mL). The radioactivity concentration was measured using a well counter (Molecular Imaging Laboratory Co. Ltd, Suita, Japan).

In two monkeys, anesthetic level was changed by altering the injection dose of propofol from 4 (baseline) to 8 and then to 12 and 16 mg/kg/h in one monkey, and to 5 and then to 7, 10, and 15 mg/kg/h in the other. In another monkey, $PaCO_2$ level was varied from 39 (baseline) to 47, and then to 33, 26, and 42 mm Hg by changing the respiratory rate. Each measurement for $^{15}O_2$ inhalation and $H_2^{15}O$ injection was initiated after at least 30 mins of applying the physiologic stimulation to achieve a steady state. All procedures were the same as those for the baseline, with the exception of the manual blood sample, which was obtained only once at 70 secs.

Before and after 6 mins of the $^{15}O_2$ inhalation, oxygen concentration in both inhaled (Fi_{O_2}, %) and end-tidal expiratory gas (Fe_{O_2}, %) was measured by the anesthetic ventilator in five out of the six monkeys. Using the respiration rate (r, per min) and the stroke volume (v, mL) indicated on the ventilator, the $BMRO_2$ (R_{O_2} mL/min) was calculated using the following equation:

$$R_{O_2} = (Fi_{O_2} - Fe_{O_2}) \cdot v \cdot r.$$

All monkeys received a PET measurement to assess the $CMRO_2$ at physiologically baseline condition. The scan protocol followed the DARG technique (Kudomi *et al*, 2005) in which a 6-mins single dynamic PET scan was performed in conjunction with the administration of dual tracers (i.e., $^{15}O_2$ followed by $H_2^{15}O$ after a 3-mins interval). PET scanner used was ECAT HR (Siemens-CTI, Knoxville, TN, USA), which provided 47 tomographic slice images for an axial field-of-view of approximately 150 mm. We performed arterial–sinus blood sampling to obtain a global OEF (OEF_{A-V}) (A–V difference approach). We sampled 0.2 mL of arterial and sinus blood simultaneously during each PET scan and measured their oxygen content (C_aO_2 and C_vO_2, respectively) (Kudomi *et al*, 2005). The OEF_{A-V} was calculated as: $OEF_{A-V} = (C_aO_2 - C_vO_2)/C_aO_2$.

With regards to the farm pigs involved in this experiment, we used existing data, which were originally obtained in one of the myocardial projects. During the study, three farm pigs were anesthetized. Anesthesia was induced by ketamine (10 mg/kg) and maintained using propofol (4 mg/kg/h). Animals were intubated and their respiration was controlled by the anesthetic ventilator. Venous blood was labeled with $^{15}O_2$ using a small artificial lung unit (Magata *et al*, 2003). $^{15}O_2$-labeled blood (222 to 700 MBq) was injected for 10 secs via anterior tibial vein. At 30 secs before this injection, arterial blood was withdrawn from the femoral artery at a rate of 0.45 mL/min using the Harvard pump and continued for 420 secs. The whole blood TAC ($A_t(t)$) was then measured with a continuous monitoring system (Kudomi *et al*, 2003). Meanwhile, we manually sampled 0.5 mL of arterial blood from the contralateral femoral artery at 30, 60, 90, 90, 120, 180, 240, and 300 secs after the $^{15}O_2$-labeled blood injection. For the analysis of sampled blood, 0.2 mL of the blood were used for measurement of the radioactivity concentration of the whole blood, and the rest of the blood sampled (~0.3 mL) was immediately centrifuged for separation to measure the plasma radioactivity ($A_{plasma}(t)$, Bq/mL). The radioactivity was measured using the well counter.

Data for rats were also originally obtained for other projects, and only the blood counts were used in this study. Anesthesia was induced with pentobarbital (50 mg/kg). A 10 mL of venous blood was labeled $^{15}O_2$ using a small artificial lung unit as described previously (Magata *et al*, 2003), and approximately 1 mL of $^{15}O_2$-labeled blood (37 to 74 MBq) was injected for 30 secs via the tail vein. Arterial blood samples of 0.1 mL each were obtained from the femoral artery at 5-secs intervals for 60 secs and 10-secs intervals for another 60 secs after the injection. Whole blood radioactivity concentration was measured using the well counter to be used as $A_t(t)$. Arterial blood samples of

0.2 mL each were obtained at 30, 60, 90, and 120 secs, and the plasma radioactivity concentration ($A_{plasma}(t)$) was measured by the well counter.

For clinical patients, the blood radioactivity concentration was obtained from previously performed PET examinations, which followed the steady-state protocol (Hirano *et al*, 1994). Each patient inhaled both $^{15}O_2$ and $C^{15}O_2$ to reach the steady state with an inhalation dose of approximately 1,200 and 500 MBq/min, respectively. Five to seven arterial blood samples were obtained during the steady state from the brachial artery. Mean values of radioactivity concentration of the whole blood and plasma, $A_t(t)$ and $A_{plasma}(t)$, respectively, were obtained for both $^{15}O_2$ and $C^{15}O_2$ PET examination.

Data Analysis

Using the blood activity data obtained from monkeys, pigs, and rats at baseline conditions, k as well as Δt, k_w and p were first determined by the 4PF approach, in which Equation 2 was applied to fit the $A_w(t)$ using the observed $A_t(t)$. Because the solubility of the oxygen is negligibly small in the plasma, we assumed that all radioactivity in plasma fraction comes from $H_2^{15}O$ and that the water content ratio of whole blood to plasma (R) does not change during measurement, which means that the kinetics of water molecules immediately reach equilibrium between the plasma and the cellular fraction (Mintun *et al*, 1984; Iida *et al*, 1993). Thus, $A_w(t)$ was obtained from the equation: $A_w(t) = A_{plasma}(t) \cdot R$, where R value was obtained from the sampled blood at the end of the scan (at which all the radioactivity in the blood can be considered as coming from $H_2^{15}O$ because inhaled $^{15}O_2$ is all metabolized).

Given that the values of Δt, k_w, and p were averages determined from 4PF for monkeys, pigs, and rats, only k was determined by fitting Equation 2 to A_w. This was calculated at various points in time, more specifically, in 30, 50, 70, 90, 110, 130, 160, and 190 secs for monkeys, in 30, 60, 90, 90, 120, 180, and 240 secs for pigs, and in 30, 60, 90, and 120 secs for rats. The optimal time point for k under the 1PF approach was determined, so that $(k_{4PF} - k_{1PF})/k_{4PF}$ reaches a minimal value. Here, k_{4PF} and k_{1PF} denote k values determined by the 4PF and 1PF approaches, respectively. The values of k in monkeys at baseline condition, together with those in pigs and rats were compared between 4PF and 1PF approaches, in which a k value from the optimal single time point was used.

In three of the monkeys, which were physiologically stimulated, k of 1PF approach was obtained using single time point of A_w. Assuming the total blood volume (V_{TB}) for monkeys as 360 mL (Lindstedt and Schaeffer, 2002), and using Hb as measured value in each experiment, k_{BM} was calculated from R_{O_2} according to Equation 7b. Then, k_{BM} obtained as: $k_{BM} = 0.00204 R_{O_2}$ was compared with k determined by 1PF.

For clinical data obtained from the steady-state (SS approach) PET examinations, Equation 6 was used to determine the k values of the SS approach for each patient, in which values of k_w and k_2 were 0.38 and 0.29 per min as obtained in a previous work by Huang *et al* (1991).

$CMRO_2$ and OEF values in monkeys at baseline condition were calculated using the RW TACs obtained by four different methods (i.e., directly measured $A_w(t)$ ($n = 6$), 4PF ($n = 6$), 1PF ($n = 6$), and BM approaches ($n = 5$)). Regions-of-interest were selected for over the whole brain, and $CMRO_2$ and OEF values were obtained in those regions-of-interest. The $CMRO_2$ values compared among the four methods mentioned above to estimate RW TACs. The Bland–Altman method was applied to analyze the agreement of OEF values between the methods. Also, OEF values were compared with OEF_{A-V}.

All data were presented as mean ± 1 standard deviation. Student's t-test was used and Pearson's regression analysis was applied to compare two variables. A probability value of < 0.05 was considered statistically significant.

Results

Figure 1 shows results from the simulation study, and shows the magnitude of errors in $CMRO_2$ calculated by the DARG method as well as errors in the parameters, k, Δt, k_w, and p. Errors in $CMRO_2$ were most sensitive to errors in k amongst all species, namely the production rate constant of RW in the arterial blood. After errors in k, errors in $CMRO_2$ were sensitive to errors in Δt. Errors in k_w and p, however, appeared to cause relatively insignificant errors in $CMRO_2$. More specifically, only 5 to 10% errors are caused in $CMRO_2$ by a change of ± 50% in k_w and p.

Figures 2A–2C show examples of the arterial whole blood curves (A_t) and RW TAC (A_w) observed in typical studies on a monkey, a pig, and a rat, respectively. The RW curves became constant after a period in all species. The rise time or appearance of the RW curves, $A_w(t)$, was significantly delayed compare to that of whole blood curve, $A_t(t)$. $A_w(t)$ curves fitted by 4PF well reproduced the measured RW curves in three species: monkeys, pigs, and rats. Table 2 summarizes values of k, Δt, k_w, and p obtained by the four parameter fitting (4PF approach), at the baseline for monkeys, pigs, and rats, and also k value obtained by the steady-state formula for clinical patients. Those comparisons showed that the k was significantly different among species ($P < 0.001$) except between pig and human subjects, and it was significantly lower in smaller animals. Likewise, Δt showed significant differences among the three species ($P < 0.001$), and it was also lower in smaller animals.

Table 3 summarizes k and $CMRO_2$ values obtained from a series of PET experiments performed on six monkeys at baseline condition, and for increased anesthesia (in two monkeys), and changed $PaCO_2$ levels (in one monkey). The best agreement of k values between 4PF and 1PF approaches was obtained from the blood sample data taken at 60, 70, and 60 secs in pigs, monkeys, and rats, respectively, and was used in the 1PF approach. With this

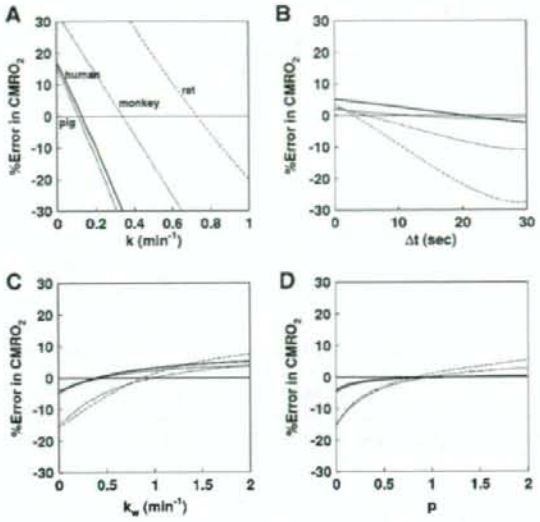

Figure 1 Error in $CMRO_2$ values due to errors in (**A**) k, (**B**) Δt, (**C**) k_w, and (**D**) p for assumed human, pig, monkey and rat. The same type of line indicates the same species. The percentage differences in the $CMRO_2$ values from the assumed true values (Table 1) were plotted as a function of the simulated value of k, Δt, k_w, and p.

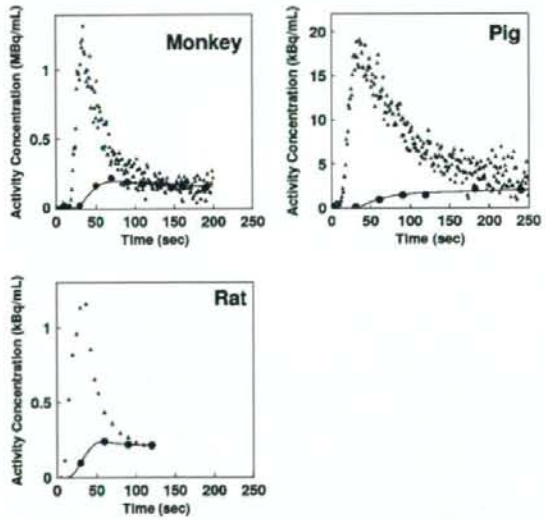

Figure 2 Representative comparison of the measured arterial whole blood and RW time activity curves for monkey, pig, and rat. Closed triangles and closed circles represent the measured whole blood and RW time activity curves, respectively. Estimated time activity curves by 4PF approach were also plotted in a solid line, and indicated a good agreement with the measured one.

optimized calibration protocol, k values were in a good agreement between 4PF and 1PF approaches. As shown in Figure 3, the regression analysis showed significant correlation for 21 animals including 6 monkeys, 3 pigs, and 12 rats ($P<0.001$), and there was no significant difference between the two variables. Figure 4 shows that k values calculated by the 1PF approach (at an optimized time) were in a good agreement with those calculated with the $BMRO_2$. Namely, the regression analysis showed significant correlation ($P<0.001$, $n=16$) and also that there was no significant difference between the two variables. Note that, in the $CMRO_2$ calculation by $BMRO_2$, k values were normalized according to the regression line shown in Figure 4. It should also be noted that calculated $CMRO_2$ values at the baseline shown in Table 3 were not significantly different among the four techniques. The average ($\pm$s.d.) values of obtained OEF were 0.53 ± 0.08, 0.52 ± 0.09, 0.54 ± 0.08, 0.54 ± 0.09, and 0.56 ± 0.04 from A–V difference, directly RW measured approach, 4PF, 1PF, and BM approaches, respectively. The Bland–Altman analysis of OEF values between from A–V difference and from others showed small over/underestimation, that is., with bias $\pm$ s.d. of -0.02 ± 0.09, 0.01 ± 0.07, 0.01 ± 0.08, and 0.02 ± 0.09, by direct RW, 4PF, 1PF, and BM approaches, respectively. Neither of the current methods (direct RW, 4PF, 1PF, and BM) was significantly different from A–V difference approach.

Discussion

Our study showed that the mathematical formula based on the physiologic model that reproduced the time-dependent concentration of RW in the arterial blood after a short-period inhalation of $^{15}O_2$ is indeed adequate. Our approach also simplified the procedures for sequential assessment of RW in $^{15}O_2$ inhalation PET studies, although previous approaches required frequent blood samples and centrifuges of each arterial blood sample. The present approach is an extension of a previous study by Iida *et al* (1993) and Huang *et al* (1991). It is essential if one intends to apply the rapid $^{15}O_2$ PET technique (Kudomi *et al*, 2005) to pharmacologic and physiologic stress studies on a wide range of species. Because the PET acquisition period can be prolonged >3 mins, statistical accuracy can be significantly improved as compared with Ohta *et al* (1992) and other researchers (Fujita *et al*, 1999; Vafaee and Gjedde, 2000; Okazawa *et al*, 2001*a*, *b*; Yamauchi *et al*, 2003; Mintun *et al*, 2002), under which to avoid effects of RW, the data acquisition period was limited only to <3 mins (Meyer *et al*, 1987; Ohta *et al*, 1992).

The present RW formula consists of three rate parameters of the production rate of RW in the arterial blood (k), and the forward and backward diffusion rate constants of RW between the blood and the peripheral tissues. The k was presumed to correspond to the oxygen metabolism in the total body system, $BMRO_2$, and was in fact shown to be

Table 2 Averaged values of k, Δt, k_w, and p for monkeys, pigs, rat, and human subjects under baseline condition

	Weight (kg)	k *(per min)*	*Δt (secs)*	k_w *(per min)*	p
Monkey	5.2 ± 0.8^a	0.34 ± 0.16^a	4.5 ± 1.4^a	0.98 ± 0.48	0.98 ± 0.30
Pig	38 ± 9^a	$0.11 \pm 0.02^{a,b}$	10.8 ± 1.8^a	0.83 ± 0.19	1.01 ± 0.26
Rat	0.30 ± 0.054^a	0.73 ± 0.16^a	2.9 ± 1.7^a	0.87 ± 0.30	0.83 ± 0.32
Human	58 ± 10^a	$0.129 \pm 0.023^{a,b}$	—	—	—

Monkey: $n = 6$; pig: $n = 3$; rat: $n = 12$; and human: $n = 231$. Measured values were obtained by 4PF for monkey, pig, rats, whereas those for human were obtained using data in a steady-state method.

[a]Denotes $P < 0.001$ for other species.

[b]Denotes that the difference was not significant in k between pig and human subjects.

Table 3 Values of k and $CMRO_2$ in the whole brain region for monkeys under physiologically baseline and stimulated conditions

ID	*Condition*	k *(per min)*			*$CMRO_2$ (mL/min per 100 g)*			
		4PF	*1PF*	*$BMRO_2$*	*Reference*	*4PF*	*1PF*	*$BMRO_2$*
1	BL	0.36	0.42	—	3.7	3.7	3.6	—
2	BL	0.62	0.66	1.24	3.0	3.3	3.4	3.4
3	BL	0.32	0.39	0.83	3.0	3.1	3.0	2.9
	(Dose of propofol)							
4	BL	0.21	0.18	0.55	2.0	2.0	2.0	1.8
	8 mg/kg/h	—	0.30	0.69	—	—	—	—
	12 mg/kg/h	—	0.23	0.52	—	—	—	—
	16 mg/kg/h	—	0.16	0.40	—	—	—	—
5	BL	0.12	0.15	0.31	2.1	2.1	2.0	1.8
	5 mg/kg/h	—	0.15	0.32	—	—	—	—
	7 mg/kg/h	—	0.16	0.35	—	—	—	—
	10 mg/kg/h	—	0.18	0.36	—	—	—	—
	15 mg/kg/h	—	0.071	0.29	—	—	—	—
	($PaCO_2$ level)							
6	BL	0.43	0.46	0.95	2.8	3.1	3.0	3.3
	47 mm Hg	—	0.20	0.64	—	—	—	—
	33 mm Hg	—	0.21	0.46	—	—	—	—
	26 mm Hg	—	0.14	0.28	—	—	—	—
	42 mm Hg	—	0.33	0.82	—	—	—	—

4PF, four parameters fitting; 1PF, one parameter fitting; $BMRO_2$, total body metabolic rate of oxygen; BL, baseline condition.
Reference: RW TAC was obtained using measured RW data at a baseline condition in all monkeys ($n = 6$). No statistically significant differences were found in $CMRO_2$ between reference and other techniques.

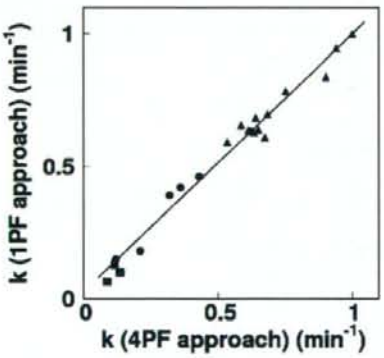

Figure 3 Comparison of the production rates of RW (k, per min) obtained by 4PF and those by 1PF. Squares, circles, and triangles correspond to pigs, monkeys, and rats, respectively. The regression line was $y = 0.97x + 0.026$ (per min) ($r = 0.98$).

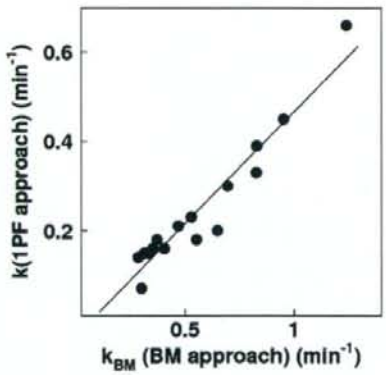

Figure 4 Comparison of the production rates of RW obtained by BM approach and those by 1PF approach in five monkeys at various anesthetic and $PaCO_2$ levels. The regression line was $y = 0.50x - 0.034$ (per min) ($r = 0.95$).

significantly correlated to $BMRO_2$, as measured from the trachea gas sampling (Figure 4). The latter two parameters (k_w and p) appeared to be consistent and did not differ across various species (Table 2). Also, change in those parameters was less sensitive in $CMRO_2$ (Figure 1). These findings suggest that the production of RW after inhalation of $^{15}O_2$ could be described only by a single parameter of k, as shown in Figure 3, although further studies are required to validate this because the method was only tested in a group with small number of subjects of particular physiologic situation (under anesthesia) and has not been applied to different populations. It is also important to note that this parameter (k) estimated from the $BMRO_2$ (i.e., BM approach) provided $CMRO_2$, which was consistent with the trachea gas samplings shown in Figure 4, and that the obtained OEF values by the approaches of 4PF, 1PF, and BM applied in the present study were not significantly different to that by A–V difference approach as revealed by Bland–Altman analysis.

The simulation study also showed that the most sensitive parameter in $CMRO_2$ was the RW production rate constant, k, followed by Δt. It was therefore suggested that k could be determined with a single blood sampling procedure using the 1PF approach, in which other parameter values were determined and fixed from results from the 4PF approach. It was further showed that k could be obtained from the BM approach as determined from oxygen concentration in the expiration gas. Both 1PF and BM approaches appeared to be robustly useful in $^{15}O_2$ PET for assessing quantitative $CMRO_2$ and CBF in clinical studies.

It is important to note that k varies significantly depending on the physiologic status even in the same species, as seen in Figure 4. According to the simulation study in Figure 1, this variation causes nonnegligible errors in $CMRO_2$, if a constant k is used. Changes in k from 0.1 to 0.6 per min causes errors in $CMRO_2$ of $\pm 30\%$ in anesthetized monkeys. Results from clinical studies, however, showed the variation in k being less. As shown in Table 2, k for clinical patients was 0.129 ± 0.023 per min, and the coefficient of variation was approximately 18%. Previous work by Huang *et al* (1991) also showed similar value with comparable variations, namely 0.131 ± 0.026 per min in six human subjects. These variations caused only $\pm 5\%$ errors in $CMRO_2$, according to the simulation shown in Figure 1. The small variation in k in clinical patients is attributed to the fact that all subjects were studied at a relatively stable condition without physiologic stimulation. However, careful attention is needed if one intends to scan the patients whose whole-body oxygen metabolism is largely changed from the baseline condition. For example, during several pharmacologically stressed (Wessen *et al*, 1997; Kaisti *et al*, 2003), exercise-induced physically stressed, and hyper- or hypothermia (Sakoh and Gjedde, 2003) conditions.

The simulation also showed that size of errors in $CMRO_2$ increased in smaller animals, where the value of k was larger. Recently, $CMRO_2$ as well as CBF have been measured in rats using a small animal PET scanner (Magata *et al*, 2003; Yee *et al*, 2006). Magata *et al* performed multiple blood samplings and plasma separation for multiple blood samples to estimate the RW in their experiment involving rats. The procedures were crucial, but have caused serious alterations of physiologic condition in heart pressure and heart rate due to large amount of blood samples for small animals. Our proposed simplified technique for estimating RW from a single blood sample or from $BMRO_2$, is essential for small animals to be able to maintain the physiologic status. The calculation of $CMRO_2$ also requires whole blood arterial TAC, which can be obtained from arterial blood samplings and could change the physiologic condition. However, such blood sampling could also be avoided by an arterial–venous bypass (Weber *et al*, 2002; Laforest *et al*, 2005), by placing a probe in femoral artery (Pain *et al*, 2004), or by a noninvasive method (Yee *et al*, 2006).

Mintun *et al* (1984) has proposed a simple procedure for RW correction based on a linear interpolation for the bolus $^{15}O_2$ inhalation 60-secs PET scan. As shown in Figure 2, the RW curve is not linear particularly in smaller animals, and a systematic error may be caused or scan duration is limited. Ohta *et al* (1992) and other investigators (Ohta *et al*, 1992; Fujita *et al*, 1999; Vafaee and Gjedde, 2000; Okazawa *et al*, 2001*a*, *b*; Yamauchi *et al*, 2003; Mintun *et al*, 2002), however, have used a technique which does not take into account the RW contribution. Only initial short-period data, namely the 3 mins after the bolus inhalation of $^{15}O_2$, were used in their approach, and thus estimated parameters suffered from statistical uncertainties. The present methodology to estimate RW in the arterial blood allows the prolongation of a PET acquisition period. The technique can also be applicable to the recently proposed sequential administration protocol of $^{15}O_2$ followed by $H_2^{15}O$ to estimate $CMRO_2$ and CBF simultaneously from a single session of a PET scan (Kudomi *et al*, 2005). This protocol, however, required a separation of a RW TAC from the whole blood TAC as showed recently (Kudomi *et al*, 2007).

The k_{BM} determined from the total body oxygen metabolism, namely the BM approach, was significantly greater than k obtained by the 4PF or the 1PF approach, by a factor 2, as shown in Figure 4. The reason is not clear, but partly attributed to the limitation of the simplified model. The body system consists of various organs which have different oxygen metabolism along with different circulation systems and with transit times. It is well known that the apparent rate constant defined with a simplified compartmental model could be underestimated as compared with an average of true rate constants, known as heterogeneity effects (Iida *et al*, 1989; Aston *et al*, 2002). This is, however, not essential.

Simply, linear correction could be applied to convert to the apparent k value as has been performed in this study. $CMRO_2$ values calculated using BM approach for the RW separation, were in good agreement with those determined with the direct measurement of RW as shown in Table 3.

The current method with modeling approach and simplified procedure provided consistent results in terms of time-dependent RW component, and consequently metabolic product of $^{15}O_2$ was separated from arterial whole blood for the $CMRO_2$ assessment in PET examination. The modeling approach to separate metabolite from authentic tracer has been showed previously for 6-[^{18}F]fluoro-L-dopa study (fdopa) (Huang *et al*, 1991). We expect that the modeling approach in conjunction with the simplified method showed in our study could be applied for various kinds of tracers, which require the separation of metabolic product such as fdopa. This approach enables us to assess parametric images for those tracers by eliminating the laborious procedures and by avoiding the amount of blood samplings, particularly for smaller animals.

In conclusion, the present RW model was feasible to reproduce RW TAC from a whole radioactivity concentration curve obtained after $^{15}O_2$ inhalation, and for a wide range of species. The simplified procedure to predict the RW TAC is of use to calculate $CMRO_2$ in smaller animals as well as clinical patients.

Acknowledgements

We acknowledge Mr N Ejima for operating the cyclotron and daily maintenance of CTI ECAT HR. We also gratefully thank Ms Atra Ardekani for her invaluable help on preparing the present paper. We also thank the staff of the Investigative Radiology, Research Institute, National Cardiovascular Center, especially, Dr T Inomata, Dr H Jino, Dr N Kawachi, and Dr T Zeniya for their assistance.

References

Aston JA, Cunningham VJ, Asselin MC, Hammers A, Evans AC, Gunn RN (2002) Positron emission tomography partial volume correction: estimation and algorithms. *J Cereb Blood Flow Metab* 22:1019–34

Eriksson L, Holte S, Bohm Chr, Kesselberg M, Hovander B (1988) Automated blood sampling system for positron emission tomography. *IEEE Trans Nucl Sci* 35:703–7

Eriksson L, Kanno I (1991) Blood sampling devices and measurements. *Med Prog Technol* 17:249–57

Fujita H, Kuwabara H, Reutens DC, Gjedde A (1999) Oxygen consumption of cerebral cortex fails to increase during continued vibrotactile stimulation. *J Cereb Blood Flow Metab* 19:266–71

Hayashi T, Watabe H, Kudomi N, Kim KM, Enmi J, Hayashida K, Iida H (2003) A theoretical model of oxygen delivery and metabolism for physiologic interpretation of quantitative cerebral blood flow and metabolic rate of oxygen. *J Cereb Blood Flow Metab* 23:1314–23

Hirano T, Minematsu K, Hasegawa Y, Tanaka Y, Hayashida K, Yamaguchi T (1994) Acetazolamide reactivity on ^{123}I-IMP single photon emission computed tomography in patients with major cerebral artery occlusive disease: correlation with positron emission tomography parameters. *J Cereb Blood Flow Metab* 14:763–70

Holden JE, Eriksson L, Roland PE, Stone-Elander S, Widen L, Kesselberg M (1988) Direct comparison of single-scan autoradiographic with multiple-scan least-squares fitting approaches to PET $CMRO_2$ estimation. *J Cereb Blood Flow Metab* 8:671–80

Huang SC, Barrio JR, Yu DC, Chen B, Grafton S, Melega WP, Hoffman JM, Satyamurthy N, Mazziotta JC, Phelps ME (1991) Modelling approach for separating blood time-activity curves in positron emission tomographic studies. *Phys Med Biol* 36:749–61

Iida H, Jones T, Miura S (1993) Modeling approach to eliminate the need to separate arterial plasma in oxygen-15 inhalation positron emission tomography. *J Nucl Med* 34:1333–40

Iida H, Kanno I, Miura S, Murakami M, Takahashi K, Uemura K (1989) A determination of the regional brain/blood partition coefficient of water using dynamic positron emission tomography. *J Cereb Blood Flow Metab* 9:874–85

Kaisti KK, Langsjo JW, Aalto S, Oikonen V, Sipila H, Teras M, Hinkka S, Metsahonkala L, Scheinin H (2003) Effects of sevoflurane, propofol, and adjunct nitrous oxide on regional cerebral blood flow, oxygen consumption, and blood volume in humans. *Anesthesiology* 99:603–13

Kudomi N, Choi C, Watabe H, Kim KM, Shidahara M, Ogawa M, Teramoto N, Sakamoto E, Iida H (2003) Development of a GSO detector assembly for a continuous blood sampling system. *IEEE Trans Nucl Sci* 50:70–3

Kudomi N, Hayashi T, Teramoto N, Watabe H, Kawachi N, Ohta Y, Kim KM, Iida H (2005) Rapid quantitative measurement of $CMRO_2$ and CBF by dual administration of ^{15}O-labeled oxygen and water during a single PET scan—a validation study and error analysis in anesthetized monkeys. *J Cereb Blood Flow Metab* 25:1209–24

Kudomi N, Watabe H, Hayashi T, Iida H (2007) Separation of input function for rapid measurement of quantitative $CMRO_2$ and CBF in a single PET scan with a dual tracer administration method. *Phys Med Biol* 52: 1893–908

Laforest R, Sharp TL, Engelbach JA, Fettig NM, Herrero P, Kim J, Lewis JS, Rowland DJ, Tai YC, Welch MJ (2005) Measurement of input functions in rodents: challenges and solutions. *Nucl Med Biol* 32:679–85

Lindstedt L, Schaeffer PJ (2002) Use of allometry in predicting anatomical and physiological parameters of mammals. *Lab Anim* 36:1–19

Magata Y, Temma T, Iida H, Ogawa M, Mukai T, Iida Y, Morimoto T, Konishi J, Saji H (2003) Development of injectable O-15 oxygen and estimation of rat OEF. *J Cereb Blood Flow Metab* 23:671–6

Meyer E, Tyler JL, Thompson CJ, Redies C, Diksic M, Hakim AM (1987) Estimation of cerebral oxygen utilization rate by single-bolus 15O2 inhalation and dynamic positron emission tomography. *J Cereb Blood Flow Metab* 7:403–14

Mintun MA, Raichle ME, Martin WR, Herscovitch P (1984) Brain oxygen utilization measured with O-15 radio-

tracers and positron emission tomography. *J Nucl Med* 25:177–87

Mintun MA, Vlassenko AG, Shulman GL, Snyder AZ (2002) Time-related increase of oxygen utilization in continuously activated human visual cortex. *Neuroimage* 16:531–7

Ohta S, Meyer E, Thompson CJ, Gjedde A (1992) Oxygen consumption of the living human brain measured after a single inhalation of positron emitting oxygen. *J Cereb Blood Flow Metab* 12:179–92

Okazawa H, Yamauchi H, Sugimoto K, Takahashi M, Toyoda H, Kishibe Y, Shio H (2001*a*) Quantitative comparison of the bolus and steady-state methods for measurement of cerebral perfusion and oxygen metabolism: positron emission tomography study using 15O-gas and water. *J Cereb Blood Flow Metab* 21:793–803

Okazawa H, Yamauchi H, Sugimoto K, Toyoda H, Kishibe Y, Takahashi M (2001*b*) Effects of acetazolamide on cerebral blood flow, blood volume, and oxygen metabolism: a positron emission tomography study with healthy volunteers. *J Cereb Blood Flow Metab* 21:1472–9

Pain F, Laniece P, Mastrippolito R, Gervais P, Hantraye P, Besret L (2004) Arterial input function measurement without blood sampling using a beta-microprobe in rats. *J Nucl Med* 45:1577–82

Sakoh M, Gjedde A (2003) Neuroprotection in hypothermia linked to redistribution of oxygen in brain. *Am J Physiol Heart Circ Physiol* 285:H17–25

Shidahara M, Watabe H, Kim KM, Oka H, Sago M, Hayashi T, Miyake Y, Ishida Y, Hayashida K, Nakamura T, Iida H (2002) Evaluation of a commercial PET tomograph-based system for the quantitative assessment of rCBF, rOEF and rCMRO2 by using sequential administration of 15O-labeled compounds. *Ann Nucl Med* 16:317–27

Temma T, Magata Y, Kuge Y, Shimonaka S, Sano K, Katada Y, Kawashima H, Mukai T, Watabe H, Iida H, Saji H (2006) Estimation of oxygen metabolism in a rat model of permanent ischemia using positron emission tomography with injectable^{15}O-O_2. *J Cereb Blood Flow Metab* 26:1577–83

Vafaee MS, Gjedde A (2000) Model of blood-brain transfer of oxygen explains nonlinear flow-metabolism coupling during stimulation of visual cortex. *J Cereb Blood Flow Metab* 20:747–54

Votaw JR, Shulman SD (1998) Performance evaluation of the Pico-Count flow-through detector for use in cerebral blood flow PET studies. *J Nucl Med* 39:509–15

Weber B, Burger C, Biro P, Buck A (2002) A femoral arteriovenous shunt facilitates arterial whole blood sampling in animals. *Eur J Nucl Med Mol Imaging* 29: 319–23

Wessen A, Widman M, Andersson J, Hartvig P, Valind S, Hetta J, Langstrom B (1997) A positron emission tomography study of cerebral blood flow and oxygen metabolism in healthy male volunteers anaesthetized with eltanolone. *Acta Anaesthesiol Scand* 41:1204–12

Yamauchi H, Okazawa H, Kishibe Y, Sugimoto K, Takahashi M (2003) The effect of acetazolamide on the changes of cerebral blood flow and oxygen metabolism during visual stimulation. *Neuroimage* 20:543–9

Yee SH, Lee K, Jerabek PA, Fox PT (2006) Quantitative measurement of oxygen metabolic rate in the rat brain using microPET imaging of briefly inhaled 15O-labelled oxygen gas. *Nucl Med Commun* 27:573–81

Parametric Renal Blood Flow Imaging Using [^{15}O]H_2O and PET

Nobuyuki Kudomi[1], Niina Koivuviita[2], Kaisa E. Liukko[1], Vesa J. Oikonen[1], Tuula Tolvanen[1], Hidehiro Iida[3], Risto Tertti[2], Kaj Metsärinne[2], Patricia Iozzo[1,4], Pirjo Nuutila[1,2]

[1] *Turku PET Centre, University of Turku, FI 20521, Turku, Finland*

[2] *Department of Medicine, University of Turku, Turku, Finland*

3 Department of Investigative Radiology, Advanced Medical-Engineering Center, National Cardiovascular Center-Research Institute, 5-7-1, Fujishirodai, Suita, Osaka, 565-8565, Japan

[4] *Institute of Clinical Physiology, National Research Council, 56100 Pisa, Italy*

Running title: RBF imaging by PET

Corresponding author

Nobuyuki Kudomi, PhD

Turku PET Centre, University of Turku

PO Box 52, FIN-20521, Turku, Finland

Phone: +358-2-313-2772

Fax: +358-2-231-8191

E-mail: nobuyuki.kudomi@tyks.fi